ACS APPLIED MATERIALS & INTERFACES

Research Article

www.acsami.org

High-Performance Supercapacitor Electrodes Based on Graphene Achieved by Thermal Treatment with the Aid of Nitric Acid

Ni Xiao,[†] Huiteng Tan,[†,‡] Jixin Zhu,[‡] Liping Tan,[†] Xianhong Rui,[†] Xiaochen Dong,[§] and Qingyu Yan[†,‡,∥,*]

[†]School of Materials Science and Engineering, Nanyang Technological University, 50 Nanyang Ave, Singapore 637819, Singapore

[‡]TUM CREATE Centre for Electromobility, Singapore 637459, Singapore

[§]Institute of Advanced Materials, Nanjing University of Technology, Nanjing 210009, China

[∥]Energy Research Institute, Nanyang Technological University, Singapore 637459, Singapore

Supporting Information

ABSTRACT: In this work, graphene materials have been prepared via thermal treatment of graphene oxides with the aid of intercalated nitric acid. The nitric acid not only favors the expansion of graphene but also facilitates the generation of pores into graphene. The specific surface area of such graphene frameworks is as high as 463 m^2/g, and the pore volume reaches up to 2.23 cm^3/g. When tested as supercapacitor electrodes, the graphene frameworks delivered an extremely high specific capacitance of ~370 F/g while simultaneously maintained an excellent energy density of 12.9 Wh/kg and power delivery of 250 W/kg in aqueous electrolyte. These performances are much better than those of the control samples prepared without the aid of nitric acid. The porous structure and large specific surface area are believed to have contributed to the high performances.

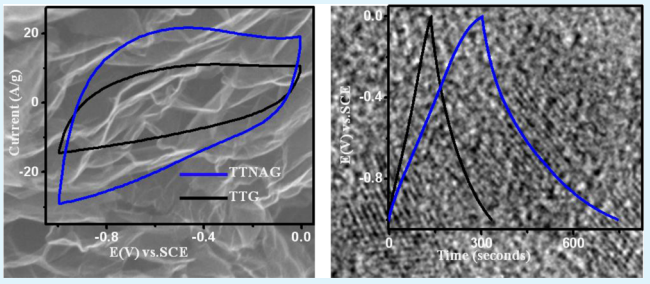

KEYWORDS: *graphene oxides, nitric acid, thermal treatment, high surface area, pores, supercapacitor*

1. INTRODUCTION

Nowadays, the growing demands for consumable portable power sources and the increasing concern about the environment issues have stimulated extensive research activities for low cost, environment friendly, and efficient energy storage/conversion devices.[1,2] Supercapacitors, also called ultracapacitors, are a class of electrochemical energy storage devices that store and release energy through charge separation at the electrochemical interface between the electrode and electrolyte.[3] Since supercapacitors could deliver high power capability and display long cycle stability, they have received considerable attention worldwide in the potential applications in portable electronics, electric vehicles, and so on.[4,5] However, the practical application of supercapacitors in industry is still limited by the lower stored energy compared with batteries.[6] Hence, increasing the energy density without sacrificing their power density and cycle life remains challenging.

Graphene, a single-atom-thick two-dimensional honeycomb nanostructure, has been proposed to be an alternative supercapacitor electrode material due to its excellent electrical conductivity, outstanding mechanical strength, superior thermal conductivity, and high theoretical surface area (~2600 m^2/g).[7,8] Currently, chemically derived graphene caught much attention toward the charge storage applications, since it could be prepared in large quantities at low cost.[9] However, the chemically derived graphene often suffers from sheet-to-sheet restacking problem during the process due to the strong interlayer van der Waals force.[10,11] This results in the great loss of its high specific surface area and limits electrolyte penetration and ion accessibility, leading to the low specific capacitance. In order to prevent restacking of graphene sheets, an effective method is to incorporate guest materials as "spacers" into the interlayer of graphene.[12−14] However, the incorporated materials such as metal oxides, metal hydroxides, and polymer would suffer gradual structural change (e.g., their degree of hydration and crystallinity) during the repeated reactions with electrolyte ions, which is detrimental to the cycling stability. On the other hand, the engineering of secondary structures (highly curved or porous structure) into graphene was proposed to be an effective way to prevent restacking of the sheets.[15−18] The crumpled/wrinkled or porous structure would increase the accessible surface area and benefit the ion transportation, favoring the excellent electrochemical performances.[19−21]

Thermal treatment is an efficient and commonly used approach for preparation of reduced graphene oxides.[22] By varying the processing conditions, graphene with different morphology and composition could be obtained.[17,23] Previous works have shown that graphene through thermal treatment at

Received: July 6, 2013
Accepted: September 17, 2013
Published: September 17, 2013

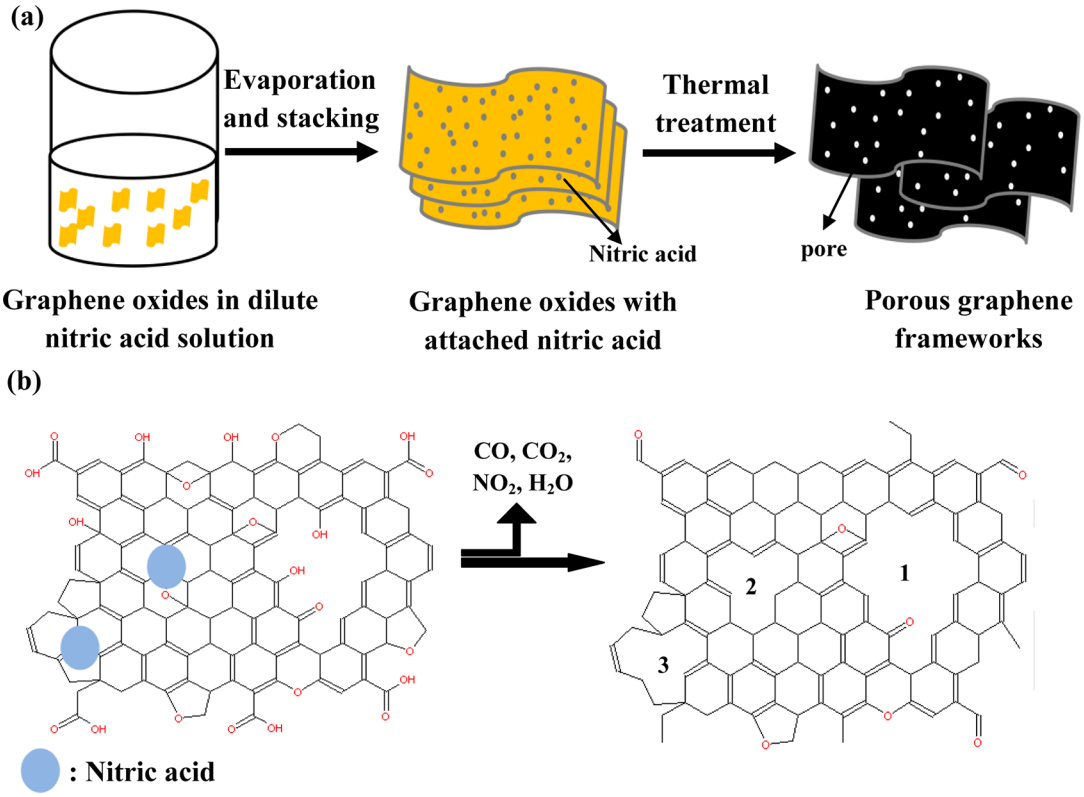

Figure 1. Schematic representations of (a) fabrication steps of TTNAG and (b) selective formation process of pores through thermal treatment.

selected conditions would exhibit good electrochemical storage performances.[24−26] For instance, corrugated graphene[27] and crumpled paper ball[28] showed improved electrochemical performances. Thermal treatment would be possible to pave a convenient route for graphene toward the supercapacitor application. However, this field is not well explored.

In this work, we prepared graphene materials through thermal treatment of graphene oxides in the presence of intercalated nitric acid. In the process, nitric acid could not only play an important role in expanding the graphene oxides but also simultaneously generate pores into the graphene due to its active chemical reaction with carbon at high temperature. The specific surface area and pore volume of the porous graphene frameworks is up to 463 m^2/g and 2.23 cm^3/g, respectively. When tested as supercapacitor electrodes, the graphene frameworks showed attractive energy storage performance, for example, ~370 F/g at a current density of 1A/g in 6 M NaOH electrolyte. This value is much higher than that of the sample without such treatment (~195 F/g at 1 A/g).

2. EXPERIMENTAL SECTION

2.1. Preparation of Graphene Oxides. Graphene oxides were synthesized from graphite powders by a modified Hummers method as reported.[29] In brief, 1 g of graphite powders, 2 g of $NaNO_3$, and 48 mL of 98% H_2SO_4 were mixed at 0 °C and continuously stirred using a magnet stirrer. $KMnO_4$ (6 g) was slowly added into above mixture below 20 °C in order to avoid overheating and explosion. Then, 40 mL of H_2O was added. After 2 h, an additional 100 mL of H_2O was added to dilute the solution, and 5 mL of 30% H_2O_2 was injected into the solution to completely react with the excess $KMnO_4$. A bright yellow solution was obtained. The resulting mixture was washed with HCl and H_2O until the pH was close to neutral, and the graphene oxides were obtained. Graphene oxides were dried in vacuum oven at 60 °C overnight.

2.2. Preparation of Thermally Treated Nitric Acid Graphene (TTNAG). Graphene oxides (100 mg) were dispersed in 50 mL of H_2O and ultrasonicated for 2 h to obtain graphene oxides solution. Concentrated nitric acid (2 mL) was added into the graphene oxides solution and ultrasonicated for 1 h. Then, the solution was dried in a Petri dish in a well-ventilated place. The nitric acid-treated graphene oxides were loaded in a quartz tube and annealed at 500 °C in a preheating furnace under mixed gas (5% hydrogen gas and 95% argon gas) for 10 min. Finally, the product was obtained.

2.3. Preparation of Thermally Treated Graphene (TTG). Graphene oxides (100 mg) were loaded in a quartz tube and annealed at 500 °C in a preheating furnace under mixed gas (5% hydrogen gas and 95% argon gas) for 10 min. Then, the sample was obtained.

2.4. Characterization. The morphology and structure of the samples were inspected by field emission scanning electron microscopy (FESEM), transmission electron microscopy (TEM), Raman spectroscopy, X-ray photoelectron spectroscopy (XPS), and nitrogen adsorption−desorption analysis. The scanning electron microscopy (SEM) images were obtained from a FESEM system (JEOL, Model JSM-7600F). TEM images of the samples were obtained using a TEM system (JEOL, model JEM 2100) operating at 200 kV. Raman spectra were obtained with a WITec CRM200 confocal Raman microscope (WITec Instruments Corp, Germany) using a 488 nm exciting radiation. Thetaprobe X-ray photoelectron spectroscopy (XPS, ESCALab 250i-XL, and Thetaprobe A1333) was used to verify the surface chemistry of samples. The nitrogen adsorption−desorption analysis was conducted at 77 K using a Micromeritics ASAP 2020 apparatus. The specific surface area was determined by the Brunauer−Emmett−Teller (BET) calculations. The pore size distribution was deduced from the adsorption branch of the isotherm based on Barrett−Joyner−Halenda (BJH) model. The elemental analysis (C, H, and N) was conducted using Elementar Vario Micro Cube.

2.5. Electrochemical Measurements. To fabricate the film electrodes, 80 wt % active material, 10 wt % carbon black, and 10 wt % polyvinylidene fluoride (PVDF) binder were mixed with N-methyl-2-pyrrolidinone (NMP). The obtained slurry was coated onto 2 × 1 cm^2

graphite papers within an area of 1 × 1 cm^2, which were then dried in vacuum at 50 °C for 12 h to remove the solvent. The mass loading of each electrode was maintained around 1 mg and the thickness was about 40 μm. The electrochemical properties and capacitance measurements of the supercapacitor electrodes were studied in a three-electrode half-cell system in 6 M NaOH electrolyte with Solartron analytical equipment (Model 1470E). Platinum wire was used as the counter electrode and Ag/AgCl as the reference electrode. Electrochemical impedance spectroscopy (EIS) measurement was carried out in the frequency from 100K to 0.01 Hz by applying 10 mV bias voltage.

3. RESULTS AND DISCUSSION

Figure 1a illustrates the preparation steps of the graphene frameworks. It has been widely reported that nitric acid could introduce defects into carbon nanotubes, cut carbon nanotubes, produce carbon dots, and form graphene nanomeshes, since it actively reacts with carbon under specified condition.[30−34] Herein, we used nitric acid as a pore generator. In the first step, the graphene oxides were dissolved in the nitric acid solution. The nitric acid could be absorbed on the surface of each layer of graphene oxides.[35] Then, the graphene oxides with attached nitric acid were dried in air at room temperature. The graphene oxides with incorporated nitric acid were obtained. It is worth noting that, in order to prevent the evaporation of nitric acid, the Petri dish containing nitric acid solution with graphene oxides was covered with prepoked tin foil and placed in a dark ventilated place. In order to prove the presence of nitric acid, we conducted the elemental analysis on the dried product. The mass fractions of carbon, hydrogen, and nitrogen are 54.18, 3.59, and 6.59%, respectively, indicating nitric acid resided in the graphene oxides. Then, the obtained dried graphene oxides with nitric acid were put into a preheated furnace at 500 °C under mixed gas (5% hydrogen and 95% argon) for 10 min. The sample after the thermal treatment was designated as thermally treated nitric acid graphene (TTNAG). In this step, the nitric acid on the surface of graphene oxides was likely to react with its neighboring carbon atoms at high temperature, especially at the defect sites (e.g., embedded mismatched pentagons and heptagons, embedded hetero atoms) to generate pores (e.g., type 2 and type 3 in Figure 1b). The gases generated may induce strong forces to expand the layers. Meanwhile some oxygen-containing functional groups (carboxyl group, hydroxyl group, carbonyl group) in graphene oxides could react with each other to release CO and CO_2, which may also favor the formation of pores (e.g., type 1 in Figure 1b). In addition, the outgassing of the CO, CO_2, NO_2, and H_2O molecules could introduce an extra force to further expand the graphene oxides and help the formation of porous frameworks. As a control experiment, thermally treated graphene (TTG) was also synthesized under the same condition without the aid of intercalated nitric acid.

Figure 2a shows the digital image of graphene oxides, TTG, and TTNAG samples with the same mass (20 mg) in the vials. From it, the expanded volume of TTNAG (20 mg) is observed to be larger than that of TTG (20 mg). This indicates the higher degree of expansion for TTNAG, which is related to the presence of nitric acid. Compared with the brown color of graphene oxides (Figure 2a-1), the black color of TTG and TTNAG indicates that the graphene oxides have been successfully reduced to graphene. In Raman spectrum (Supporting Information Figure S1), the increased intensity ratio of D band to G band (I_D/I_G) for TTNAG and TTG, compared to that of graphene oxides, also proves it.[36,37]

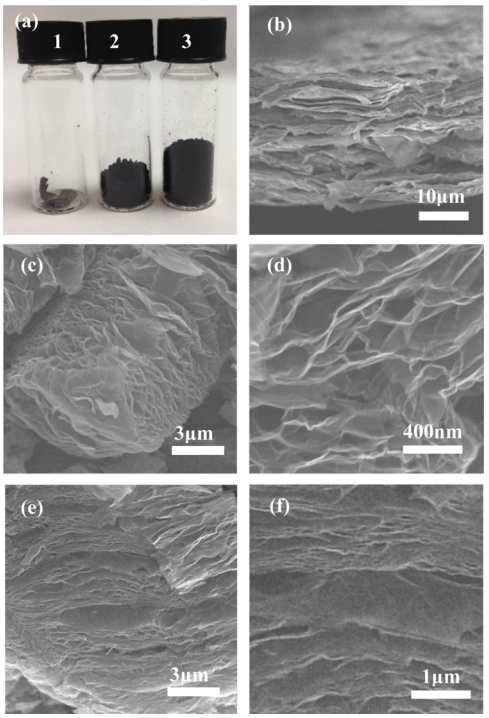

Figure 2. (a) Digital image of graphene oxides, TTG, and TTNAG, marked by 1, 2, and 3, separately. SEM images of (b) graphene oxides, (c, d) TTNAG, and (e, f) TTG.

Additionally, XPS was conducted to further investigate these samples (Supporting Information Figure S2). The increased C/O ratios confirm that TTNAG and TTG are reduced successfully. In the C1s XPS spectrum, the fitted peaks centered at 284.5, 286.7, 288.3, and 289.1 eV are assigned to C—C, C—O, C═O, and O═C—O, respectively.[36,38] The relative ratios of different surface functionalities are summarized in their insets. It is worth noting that a small amount of oxygen-containing functional groups are still in TTNAG and TTG.

The morphologies of graphene oxides, TTNAG, and TTG were further investigated by SEM. The SEM image of crossing section of graphene oxides (Figure 2b) indicates these sheets are stacked. For TTNAG (Figure 2c), the stacked graphene oxides are effectively exfoliated to separated sheets with interconnected 3D porous structure. The pore sizes ranging from 30 to 300 nm are clearly visible (Figure 2d). While for TTG (Figure 2e, f), 3D interconnected porous structure could also be observed, which is related to the outgassing of CO, CO_2, and H_2O, releasing from the reduced oxygen-containing functional groups during the thermal process. However, compared with TTNAG, it is not so fully expanded. These SEM results indicate that nitric acid plays an important role in expanding the graphene.

Figure 3a shows the low-magnification TEM image of TTNAG, in which the transparent ultrathin sheets with wrinkles could be observed. The high-magnification TEM images (Figure 3b, c) exhibit pores with different sizes in the TTNAG samples. Some of the pores are marked in red circles. We speculate that besides removal of functional groups induced pores, individual nitric acid molecule, anchored separately onto the layers of graphene oxides, could also react with the neighboring carbon and therefore generate pores. These micropores could be clearly observed in Figure 3c. For TTG, the TEM images show the transparent sheets with wrinkles

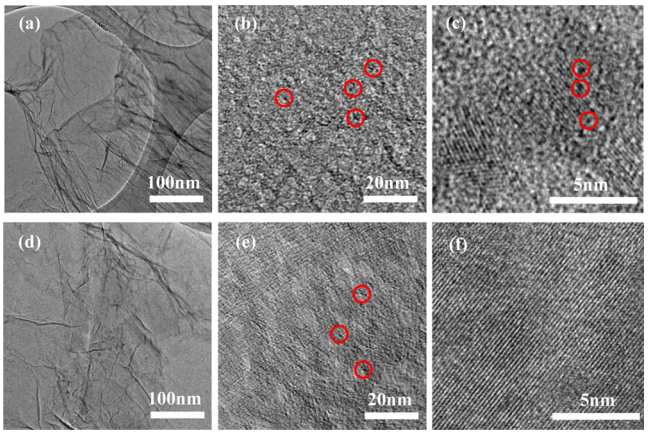

Figure 3. Low-magnification (a) and high-magnification (b, c) TEM images of TTNAG. Low- magnification (d) and high-magnification (e, f) TEM images of TTG. Some pores are marked by the red circles.

(Figure 3d), but there are fewer pores in the thin nanosheets than TTNAG (Figure 3e, f). In this case, lack of the nitric acid-induced pores, the quantity of the pores is expected to be less than that of TTNAG, although the thermal treatment could also reduce some of the oxygen-containing functional groups to form pores.

In order to further confirm the detailed porous structure in the TTNAG sample, we conducted nitrogen adsorption−desorption measurements. As shown in Figure 4a, the isotherms of TTNAG and the control sample TTG exhibit the characteristics of type IV with a distinct type H3 hysteresis loop in the P/P_o range of 0.45−1.00 based on the standard definition of International Union of Pure and Applied Chemistry (IUPAC). It implies the presence of mesopores and macropores raised from the aggregation of sheets in the frameworks. However, only for the isotherm of TTNAG, a sharp rise at low P/P_o (~0.01) at the initial region of the isotherms can be observed, indicating a small amount of micropores existing in the framework. These pores may be related to the reaction of nitric acid and the neighboring carbon atoms. The specific surface area of TTNAG and TTG is 463 and 215 m^2/g, respectively, based on the Brunauer−Emmett−Teller (BET) analysis. The increased surface area may originate from the higher degree of expansion and increased number of pores in TTNAG. The pore volume ranging from 1.7 to 100 nm shows a higher value of 2.23 cm^3/g for TTNAG than that for TTG (e.g., 1.01 cm^3/g). Barrett−Joyner−Halenda (BJH) pore size distributions of the samples (Figure 4b) also show the significant higher incremental pore volume ranging from around 2 to 100 nm for TTNAG than TTG.

The large surface area and porous structure make TTNAG a potential excellent material toward supercapacitor application. So, we measured the charge storage performances of TTNAG electrodes with a three-electrode system in 6 M KOH aqueous solution. For comparison, we also evaluated the charge storage performances of electrodes made from TTG.

Figure 5a demonstrates the representative cyclic voltammogram (CV) curves of TTNAG and TTG electrodes between 0 and −1 V at a scan rate of 100 mV/s. These CV curves exhibit a quasi-rectangular shape, showing the electrostatic characteristic of electric double-layer capacitors (EDLC). Meanwhile, small humps could be observed, which could be attributed to the presence of oxygen-containing functional groups. The larger area of the rectangular curve of TTNAG electrodes indicates the higher specific capacitance. The detailed CV curves of the TTNAG and TTG samples at various scan rates (5−100 mV/S) were also plotted (Supporting Information Figure S3a, b). Figure 5b shows the galvanostatic charge/discharge curves of the TTNAG and TTG electrodes at a current density of 1 A/g. The detailed charge/discharge curves of the electrodes were also measured at different current densities (1, 2, 5, 10, 15, 20 A/g) (Supporting Information Figure S3c, d). The specific capacitances of the electrodes, Cs, were calculated from the galvanostatic charge/discharge curves using the following equation:

$$\mathrm{Cs} = \frac{I}{\left(\frac{\Delta E}{\Delta t}\right)m}$$

Where I is the discharge current, $(\Delta E/\Delta t)$ is the average slope of the discharge curve after the IR drop, Δt is discharge time, and m is active mass. The calculated specific capacitances of the TTNAG electrodes are 370, 290, 250, 210, 190 F/g at current densities of 1, 2, 5, 10, 15 A/g, respectively (Figure 5c). Even at a high current density of 20 A/g, the TTNAG electrodes could still deliver a specific capacitance of 180 F/g. As a comparison, the TTG electrodes exhibit lower specific capacitances of 195, 150, 125, 100, 90, 80 F/g at current densities of 1, 2, 5, 10, 15, 20 A/g (Figure 5c), respectively. The specific capacitance of the TTNAG electrodes (370 F/g at current density of 1 A/g) is considered to be excellent as compared to some of the state-of-

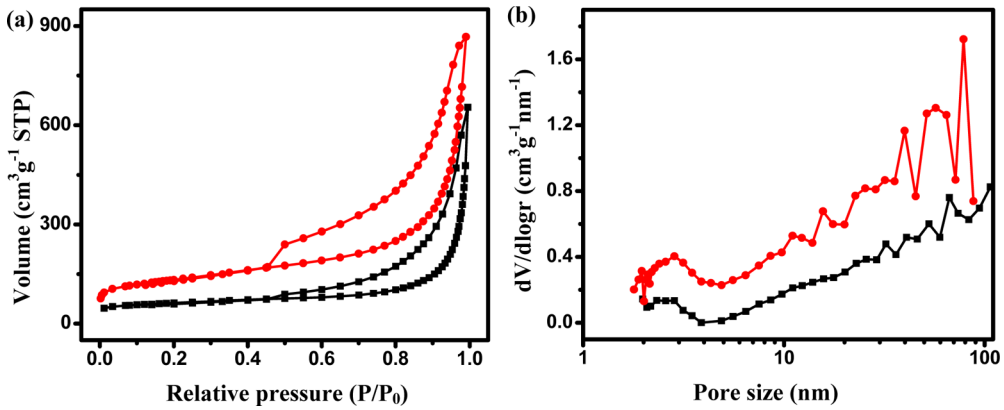

Figure 4. (a) Nitrogen adsorption−desorption isotherms and (b) BJH adsorption pore size distribution of TTNAG and TTG. (TTNAG, red line; TTG, black line.)

dx.doi.org/10.1021/am402686r | ACS Appl. Mater. Interfaces 2013, 5, 9656−9662

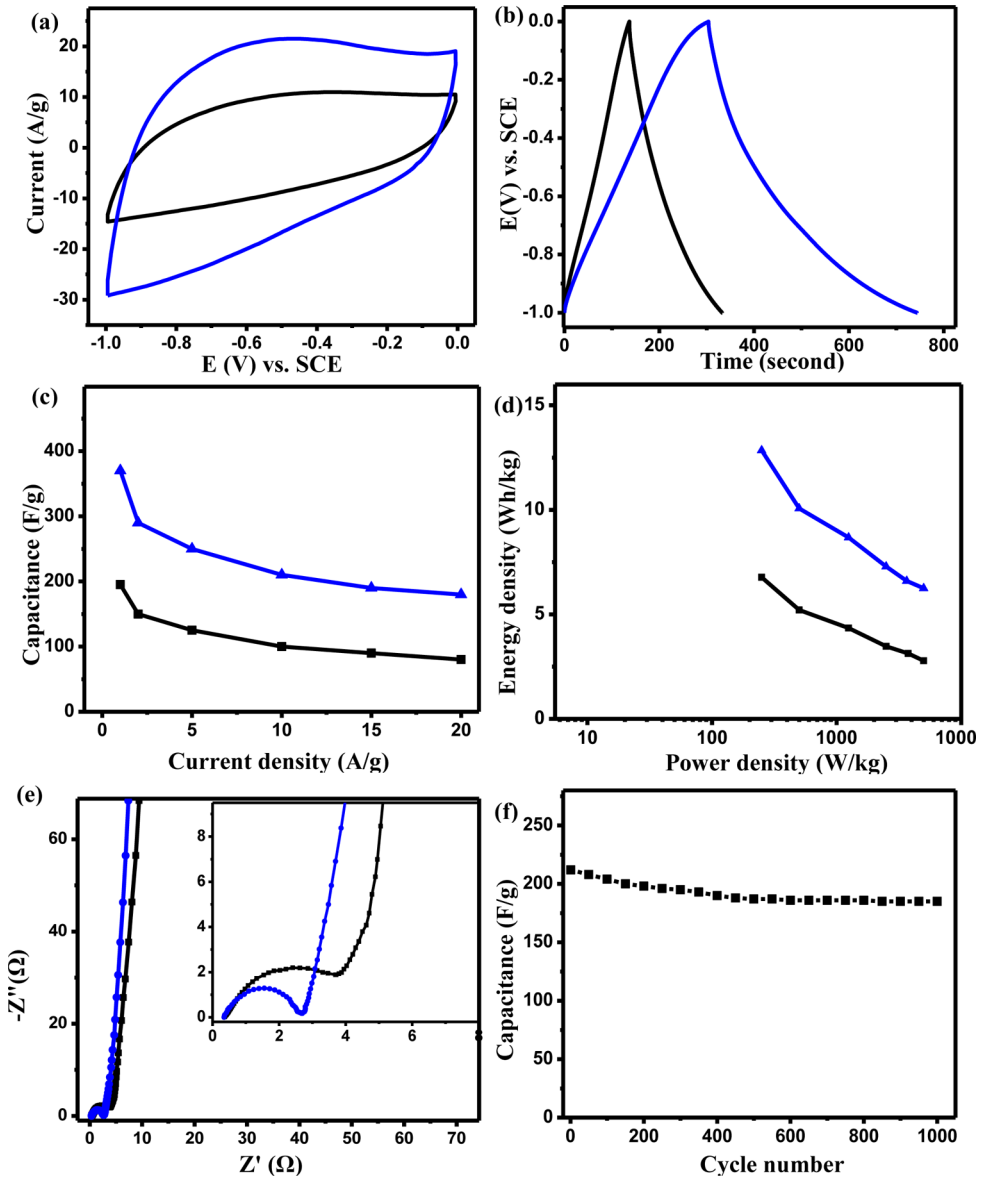

Figure 5. (a) CV curves of TTNAG and TTG at a scan rate of 100 mV/s. (b) Galvanostatic charge/discharge curves of TTNAG and TTG at current density of 1 A/g. (c) Specific capacitance versus different current density. (d) Energy density versus power density of TTNAG and TTG. (e) Nyquist plots of TTNAG and TTG. (TTNAG in blue line, TTG in black line). (f) Cycling performance of TTNAG electrode at a current density of 10 A/g.

the-art values, for example, nitrogen-doped porous carbon nanofibers (202 F/g),[39] functionalized graphene by solvothermal method (276 F/g),[40] and active carbon (100 F/g).[41]

Figure 5d demonstrates the Ragone plots of the samples, showing the relationship between the energy density and power density. The energy densities (E) and power densities (P) were calculated derived from the discharge curves according to the following equations:

$$E = \frac{1}{2}\left(\frac{Cs}{4}\right)V^2$$

$$P = \frac{E}{t}$$

where Cs is the specific capacitance (in a three-electrode system, one-fourth of the specific capacitance of a single electrode is used),[25,27,42] V is the applied voltage, and t is the discharge time respectively. At a power density of 250 W/kg, the energy density of TTNAG can reach 12.9 Wh/kg, which is much higher than that of TTG (6.8 Wh/kg). This energy density is also higher than the values reported for ordered mesoporous carbons (9.4 Wh/kg),[43] nitrogen and boron codoped 3D graphene (8.7 Wh/kg),[44] and corrugated graphene (7.6 Wh/kg)[27] in aqueous electrolytes.

Electrochemical impedance spectroscopy was used to study the kinetic features of the ion diffusion in TTNAG and TTG electrodes. The x-axis intercepts at high frequency in the Nyquist plots (Figure 5e) for TTNAG and TTG are 0.34 and 0.36, indicating the internal or equivalent series resistances of the electrodes are almost the same.[27] The radius of the semicircle at high frequency for TTNAG is shorter than that of TTG, illustrating the smaller charge transfer resistance. The shorter Warbug-type line (45° portion of the curve) for TTNAG also signifies the faster kinetics of ion transfer.[45]

dx.doi.org/10.1021/am402686r | ACS Appl. Mater. Interfaces 2013, 5, 9656−9662

To evaluate the electrochemical stability of the TTNAG electrodes, the galvanostatic charge/discharge process was conducted at a current density of 10 A/g for 1000 cycles. As shown in Figure 5f, after 1000 times of cycling, the capacitance still maintains 185 F/g, showing a prominent performance in durability and stability. The morphology of TTNAG electrodes after charge/discharge cycling test was also investigated using SEM. There is no significant structural change after 1000 cycles and some of the pores could still be observed (Supporting Information Figure S4), which contributes to the good stability.

In TTNAG, the porous structure and a large specific surface area are regarded to contribute to the high electrochemical performances of TTNAG. The highly interconnected porous structure could decrease the diffusion distances and accelerate the charge transportation. The large accessible surface area can absorb electrolyte ions effectively and increase the assembled ions on the surface of electrodes. The increased edge defects caused by the pores were also reported to have a positive effect on the electrochemical capacitances.[46]

In order to investigate the effect of the concentration of the nitric acid, we added different amount of nitric acid (e.g., 1, 2, 4 mL) into the solution containing graphene oxides. After the same drying process and thermal treatment, there were no obvious differences in surface areas and pore volumes for these samples (Supporting Information Table S1). The related nitrogen adsorption−desorption isotherms are shown in Supporting Information Figure S5. We propose that the adsorption of the nitric acid molecules on the surface of graphene is not stable, which may be easily desorbed during drying process. The electrochemical performances were also tested for these samples. The CV and charge/discharge profiles show no obvious differences for these samples (Supporting Information Figure S6).

4. CONCLUSION

We have prepared graphene frameworks via thermal treatment of graphene oxides assisted with the intercalated nitric acid. When tested as an electrode material for supercapacitor, such graphene frameworks exhibited excellent electrochemical performance (e.g., specific capacitance 370 F/g at 1 A/g and 88% retention rate after 1000 cycles). The good performances are attributed to the easy penetration of the electrolyte ions and effective absorbing sites for these ions due to the porous structures and large surface areas of the frameworks. Prospectively, such architecture would also be beneficial for catalysis and drug delivery applications.

■ ASSOCIATED CONTENT

Supporting Information

Raman and XPS data of graphene oxides, TTG, and TTNAG; additional electrochemical performances of TTG and TTNAG; SEM images of TTNAG electrodes after stability test; nitrogen adsorption−desorption isotherms, CV, and charge−discharge curves, surface areas and pore volumes of thermally treated graphene oxides treated with different amount of nitric acid. This material is available free of charge via the Internet at http://pubs.acs.org.

■ AUTHOR INFORMATION

Corresponding Author

*E-mail: AlexYan@ntu.edu.sg.

Notes

The authors declare no competing financial interest.

■ ACKNOWLEDGMENTS

The authors gratefully acknowledge NRF2009EWT-CERP001-026 (Singapore), A*STAR SERC Grant No. 1021700144, Singapore MPA 23/04.15.03 grant, and Singapore National Research Foundation under CREATE program: EMobility in Megacities.

■ REFERENCES

(1) Arico, A. S.; Bruce, P.; Scrosati, B.; Tarascon, J. M.; Van Schalkwijk, W. *Nat. Mater.* **2005**, *4*, 366−377.
(2) Reddy, A. L. M.; Gowda, S. R.; Shaijumon, M. M.; Ajayan, P. M. *Adv. Mater.* **2012**, *24*, 5045−5064.
(3) Frackowiak, E.; Beguin, F. *Carbon* **2001**, *39*, 937−950.
(4) Simon, P.; Gogotsi, Y. *Nat. Mater.* **2008**, *7*, 845−854.
(5) Rui, X. H.; Lu, Z. Y.; Yin, Z. Y.; Sim, D. H.; Xiao, N.; Lim, T. M.; Hng, H. H.; Zhang, H.; Yan, Q. Y. *Small* **2013**, *9*, 716−721.
(6) Dai, L.; Chang, D. W.; Baek, J.-B.; Lu, W. *Small* **2012**, *8*, 1130−1166.
(7) Huang, Y.; Liang, J.; Chen, Y. *Small* **2012**, *8*, 1805−1834.
(8) Stoller, M. D.; Park, S.; Zhu, Y.; An, J.; Ruoff, R. S. *Nano Lett.* **2008**, *8*, 3498−3502.
(9) Segal, M. *Nat. Nano* **2009**, *4*, 612−614.
(10) Yang, X. W.; Zhu, J. W.; Qiu, L.; Li, D. *Adv. Mater.* **2011**, *23*, 2833−2838.
(11) Si, Y.; Samulski, E. T. *Chem. Mater.* **2008**, *20*, 6792−6797.
(12) Wu, Q.; Xu, Y. X.; Yao, Z. Y.; Liu, A. R.; Shi, G. Q. *ACS Nano* **2010**, *4*, 1963−1970.
(13) Li, Z.-F.; Zhang, H.; Liu, Q.; Sun, L.; Stanciu, L.; Xie, J. *ACS Appl. Mater. Interfaces* **2013**, *5*, 2685−2691.
(14) Lei, Z.; Shi, F.; Lu, L. *ACS Appl. Mater. Interfaces* **2012**, *4*, 1058−1064.
(15) Qiu, L.; Liu, J. Z.; Chang, S. L. Y.; Wu, Y.; Li, D. *Nat. Commun.* **2012**, *3*, 1241.
(16) Chen, Z.; Ren, W.; Gao, L.; Liu, B.; Pei, S.; Cheng, H.-M. *Nat. Mater.* **2011**, *10*, 424−428.
(17) Luo, J. Y.; Jang, H. D.; Sun, T.; Xiao, L.; He, Z.; Katsoulidis, A. P.; Kanatzidis, M. G.; Gibson, J. M.; Huang, J. X. *ACS Nano* **2011**, *5*, 8943−8949.
(18) Xu, Y. X.; Sheng, K. X.; Li, C.; Shi, G. Q. *ACS Nano* **2010**, *4*, 4324−4330.
(19) Gao, H.; Xiao, F.; Ching, C. B.; Duan, H. *ACS Appl. Mater. Interfaces* **2012**, *4*, 2801−2810.
(20) El-Kady, M. F.; Strong, V.; Dubin, S.; Kaner, R. B. *Science* **2012**, *335*, 1326−1330.
(21) Zhu, Y.; Murali, S.; Stoller, M. D.; Ganesh, K. J.; Cai, W.; Ferreira, P. J.; Pirkle, A.; Wallace, R. M.; Cychosz, K. A.; Thommes, M.; Su, D.; Stach, E. A.; Ruoff, R. S. *Science* **2011**, *332*, 1537−1541.
(22) Kuila, T.; Mishra, A. K.; Khanra, P.; Kim, N. H.; Lee, J. H. *Nanoscale* **2013**, *5*, 52−71.
(23) Park, O.-K.; Hahm, M. G.; Lee, S.; Joh, H.-I.; Na, S.-I.; Vajtai, R.; Lee, J. H.; Ku, B.-C.; Ajayan, P. M. *Nano Lett.* **2012**, *12*, 1789−1793.
(24) Zhang, H.; Bhat, V. V.; Gallego, N. C.; Contescu, C. I. *ACS Appl. Mater. Interfaces* **2012**, *4*, 3239−3246.
(25) Chen, C.-M.; Zhang, Q.; Yang, M.-G.; Huang, C.-H.; Yang, Y.-G.; Wang, M.-Z. *Carbon* **2012**, *50*, 3572−3584.
(26) Wen, Z.; Wang, X.; Mao, S.; Bo, Z.; Kim, H.; Cui, S.; Lu, G.; Feng, X.; Chen, J. *Adv. Mater.* **2012**, *24*, 5610−5616.
(27) Yan, J.; Liu, J.; Fan, Z.; Wei, T.; Zhang, L. *Carbon* **2012**, *50*, 2179−2188.
(28) Luo, J.; Jang, H. D.; Huang, J. *ACS Nano* **2013**, *7*, 1464−1471.
(29) Zhao, J. P.; Pei, S. F.; Ren, W. C.; Gao, L. B.; Cheng, H. M. *ACS Nano* **2010**, *4*, 5245−5252.
(30) Wu, Y. P.; Jiang, C.; Wan, C.; Holze, R. *J. Power Sources* **2002**, *111*, 329−334.

(31) Zhang, X.; Sreekumar, T. V.; Liu, T.; Kumar, S. *J. Phys.Chem. B* **2004**, *108*, 16435−16440.
(32) Wang, Q. L.; Zheng, H. Z.; Long, Y. J.; Zhang, L. Y.; Gao, M.; Bai, W. J. *Carbon* **2011**, *49*, 3134−3140.
(33) Kang, Y. R.; Li, Y. L.; Deng, M. Y. *J. Mater. Chem.* **2012**, *22*, 16283−16287.
(34) Wang, X.; Jiao, L.; Sheng, K.; Li, C.; Dai, L.; Shi, G. *Sci. Rep.* **2013**, *3*, 1996.
(35) Kasry, A.; Kuroda, M. A.; Martyna, G. J.; Tulevski, G. S.; Bol, A. A. *ACS Nano* **2010**, *4*, 3839−3844.
(36) Stankovich, S.; Dikin, D. A.; Piner, R. D.; Kohlhaas, K. A.; Kleinhammes, A.; Jia, Y.; Wu, Y.; Nguyen, S. T.; Ruoff, R. S. *Carbon* **2007**, *45*, 1558−1565.
(37) Dong, X. C.; Su, C. Y.; Zhang, W. J.; Zhao, J. W.; Ling, Q. D.; Huang, W.; Chen, P.; Li, L. J. *Phys. Chem. Chem. Phys.* **2010**, *12*, 2164−2169.
(38) Lei, Z.; Lu, L.; Zhao, X. S. *Energy Environ. Sci.* **2012**, *5*, 6391−6399.
(39) Chen, L.-F.; Zhang, X.-D.; Liang, H.-W.; Kong, M.; Guan, Q.-F.; Chen, P.; Wu, Z.-Y.; Yu, S.-H. *ACS Nano* **2012**, *6*, 7092−7102.
(40) Lin, Z.; Liu, Y.; Yao, Y.; Hildreth, O. J.; Li, Z.; Moon, K.; Wong, C.-p. *J. Phys. Chem. C* **2011**, *115*, 7120−7125.
(41) Qu, D.; Shi, H. *J. Power Sources* **1998**, *74*, 99−107.
(42) Nam, K.-W.; Lee, C.-W.; Yang, X.-Q.; Cho, B. W.; Yoon, W.-S.; Kim, K.-B. *J. Power Sources* **2009**, *188*, 323−331.
(43) Xing, W.; Qiao, S. Z.; Ding, R. G.; Li, F.; Lu, G. Q.; Yan, Z. F.; Cheng, H. M. *Carbon* **2006**, *44*, 216−224.
(44) Wu, Z.-S.; Winter, A.; Chen, L.; Sun, Y.; Turchanin, A.; Feng, X.; Müllen, K. *Adv. Mater.* **2012**, *24*, 5130−5135.
(45) Xu, Z.; Li, Z.; Holt, C. M. B.; Tan, X.; Wang, H.; Amirkhiz, B. S.; Stephenson, T.; Mitlin, D. *J. Phys. Chem. Lett.* **2012**, *3*, 2928−2933.
(46) Song, W.; Ji, X.; Deng, W.; Chen, Q.; Shen, C.; Banks, C. E. *Phys. Chem. Chem. Phys.* **2013**, *15*, 4799−4803.